



ELSEVIER

Journal of Alloys and Compounds xxx (2005) xxx–xxx

Journal of  
ALLOYS  
AND COMPOUNDS

www.elsevier.com/locate/jallcom

# Formation of boride layers at the Fe–10% Cr alloy–boron interface

V.I. Dybkov<sup>a,\*</sup>, W. Lengauer<sup>b</sup>, K. Barmak<sup>c</sup><sup>a</sup> Department of Physical Chemistry of Inorganic Materials, I.V. Frantsevich Institute for Problems of Materials Science, Krzhyzhanivsky Str 3, 03180 Kyiv, Ukraine<sup>b</sup> Institute for Chemical Technologies and Analytics, Vienna University of Technology, 1060 Vienna, Austria<sup>c</sup> Department of Materials Science and Engineering, Carnegie Mellon University, Pittsburgh, PA 15213, USA

Received 24 January 2005; accepted 16 February 2005

## Abstract

Two boride phases FeB and Fe<sub>2</sub>B were found to form as separate layers at the interface between an Fe–10% Cr alloy and boron at 850–950 °C and reaction times up to 12 h, with Cr content around 6 at.% in FeB and 7 at.% in Fe<sub>2</sub>B. The characteristic feature of both layers is a pronounced texture. The strongest reflections are {002} and {020} for the orthorhombic FeB phase and {002} for the tetragonal Fe<sub>2</sub>B phase. Formation of boride layers is sequential rather than simultaneous, with the Fe<sub>2</sub>B layer occurring first. Their diffusional growth kinetics are close to parabolic and can alternatively be described by a system of two non-linear differential equations, also producing a good fit to the experimental data. Annealing of a borided Fe–Cr sample in the absence of boriding media results in disappearance of the FeB layer and then in disintegration of the Fe<sub>2</sub>B layer into separate grains. Grain-boundary diffusion plays a significant role in this process. Microhardness values are 13.0 GPa for the FeB layer, 11.8 GPa for the Fe<sub>2</sub>B layer and 1.3 GPa for the Fe–10% Cr alloy base. The abrasive wear resistance of the (Fe, Cr)B layer is at least 10 times greater than that of the alloy base. The (Fe, Cr)<sub>2</sub>B layer yields about a 5-fold increase in wear resistance of an Fe–10% Cr alloy.

© 2005 Published by Elsevier B.V.

**Keywords:** Fe–10% Cr alloy; Boron; Boride layers; Phase identity; Chemical composition; Growth kinetics; Abrasive wear resistance

## 1. Introduction

Boriding is one of the thermochemical surface treatments used to improve service characteristics (hardness, mechanical and corrosive wear resistance, etc.) of steels, metals and alloys [1–3]. Iron borides Fe<sub>2</sub>B and FeB are known to exist in the Fe–B binary system [4–7]. Therefore, with iron, its alloys and steels, either one-phase or two-phase coatings can be obtained, depending on boriding techniques employed and temperature–time conditions of a boriding procedure.

It is worth noting that even if three or more compounds exist in the metal–boron binary system, in most cases only two of them form separate layers at the interface between

reacting phases [8]. This contradicts diffusional considerations [9] predicting the simultaneous formation and subsequent parabolic growth of the layers of all compounds of any binary system, whatever their number, but agrees with a physicochemical viewpoint [10], according to which one or two layers can occur and grow simultaneously under conditions of diffusion control, with other compound layers being absent for kinetic reasons.

The properties of boride coatings are to a large extent dependent on the amount of alloying elements and impurities present in the base material. In the case of materials of complicated chemical composition, it is not so easy to separate the effect of a particular element from that of others. Therefore, experiments with binary alloys are desirable. In this work, the results of the experimental investigation of the interaction of a Fe–10% Cr alloy with boron at 850–950 °C are presented.

\* Corresponding author. Tel.: +38 44 4243090; fax: +38 44 4242131.

E-mail address: vdybkov@ukr.net (V.I. Dybkov).

## 2. Experimental

### 2.1. Materials and specimens

The materials used included high-purity iron powder (99.98% Fe), electrolytic-grade chromium platelets (99.98% Cr), amorphous boron and analytical-grade  $\text{KBF}_4$ . Initially, the boron powder contained 98.3% B, 0.04% C, 1.6% O and insignificant amounts of Si, Cu, Mg (<0.01% each) and Fe (<0.001%). Before the boriding experiments, the powder was first heated slowly in vacuum up to 1450 °C and then calcined at this temperature for 2 h in an atmosphere of argon at a pressure of  $2.5 \times 10^4$  Pa to remove volatile oxides.  $\text{KBF}_4$  was preliminary dried in steps at 95, 110, 130 and 170 °C (24 h at each temperature).

Cylindrical rods of a Fe–10% Cr alloy, about 13 mm in diameter and 100 mm long, were prepared by arc-melting of appropriate metals under argon, with subsequent casting of the melts into water-cooled copper crucibles. The rods were annealed to ensure their homogenization at a temperature of 1100 °C for 2 h in an argon atmosphere at a pressure of  $2.5 \times 10^4$  Pa. From these, Fe–Cr alloy specimens in the form of tablets, 11.28 mm diameter and 5.5 mm high, were machined. Flat sides (1  $\text{cm}^2$  area) of the tablets were ground and polished mechanically.

### 2.2. Experimental methods

The vacuum device VPBD-2S employed for boriding (boronizing) the metals, alloys and steels consists of a high-vacuum chamber with a molybdenum-sheet electric-resistance furnace (temperatures up to 1600 °C) and a control panel (Fig. 1). The experiment was carried out in an alumina crucible, 13 mm inner diameter and 40 mm high.

An iron–chromium alloy tablet was embedded into a mixture of boron powder with 5%  $\text{KBF}_4$  as an activator. This



Fig. 1. The vacuum device VPBD-2S for boriding (boronizing) the metals, alloys and steels.

Table 1

Comparison of literature and experimental X-ray data ( $d$ -spacing and peak intensities) for the FeB phase formed at the interface between a Fe–10% Cr alloy and boron at 950 °C and a reaction time of 21,600 s (6 h)

$hkl$	Literature data [11]		Experimental data	
	$d$ (nm)	$I^a$	$d$ (nm)	$I$
1 1 0	0.326	m	0.3255	w
0 2 0	0.275	s	0.2746	s
1 0 1	0.240	s	0.2380	vw
1 2 0	0.228	s	0.2271	s
1 1 1	0.219	vs	0.2181	w
2 0 0; 0 2 1	0.201	vs	0.2006	vs
2 1 0	0.190	vs	0.1903	vs
1 2 1	0.181	s	0.1801	s
1 3 0	0.167	s	0.1670	s
2 1 1	0.160	s	0.1597	vw
0 0 2	0.148	m	0.1489	vw
0 2 2	0.1303	m	0.1302	s
0 4 1	0.1249	m	0.1245	m
1 2 2	0.1239	vs	0.1233	s
3 1 1	0.1199	m	0.1197	w
2 1 2	0.1166	vs	0.1160	m

<sup>a</sup> Intensity: vw—very weak, w—weak, m—medium, s—strong, vs—very strong.

amount of  $\text{KBF}_4$  appears to be optimum [1,8]. The mixture was then slightly pressed, and a load of 8.5 g (a low-carbon steel cylinder) was placed on top. The crucible was closed with a low-carbon steel lid and placed into a steel-sheet holder, mounted to a guide rod capable of moving in the vertical direction.

The chamber was pumped to a pressure of about 10 Pa and filled with high-purity argon (99.999 vol.% Ar). This procedure was repeated twice. Then, the chamber was again pumped and filled with argon at a pressure of  $2.5 \times 10^4$  Pa, and heating was started. During heating, the crucible with its contents was in the cold zone above the furnace. After the required temperature in the range of 850–950 °C had been reached in the furnace, the crucible, pre-heated to about 400 °C, was moved into its middle part. After an initial drop,

Table 2

Comparison of literature and experimental X-ray data ( $d$ -spacing and peak intensities) for the  $\text{Fe}_2\text{B}$  phase formed at the interface between a Fe–10% Cr alloy and boron at 950 °C and a reaction time of 21,600 s (6 h)

$hkl$	Literature data [11]		Experimental data	
	$d$ (nm)	$I^a$	$d$ (nm)	$I$
2 0 0	0.256	vw	0.2549	vw
0 0 2	0.212	w	0.2113	vs
2 1 1	0.201	vs	0.2018	w
1 1 2	0.183	m	0.1831	w
2 0 2	0.163	m	0.1623	w
3 1 0	0.161	m	0.1611	vw
2 2 2	0.1371	w	0.1377	vw
4 0 0	0.1277	m	0.1278	vw
1 2 3	0.1202	s	0.1204	w
4 1 1	0.1187	m	0.1185	m

<sup>a</sup> Intensity: vw—very weak, w—weak, m—medium, s—strong, vs—very strong.

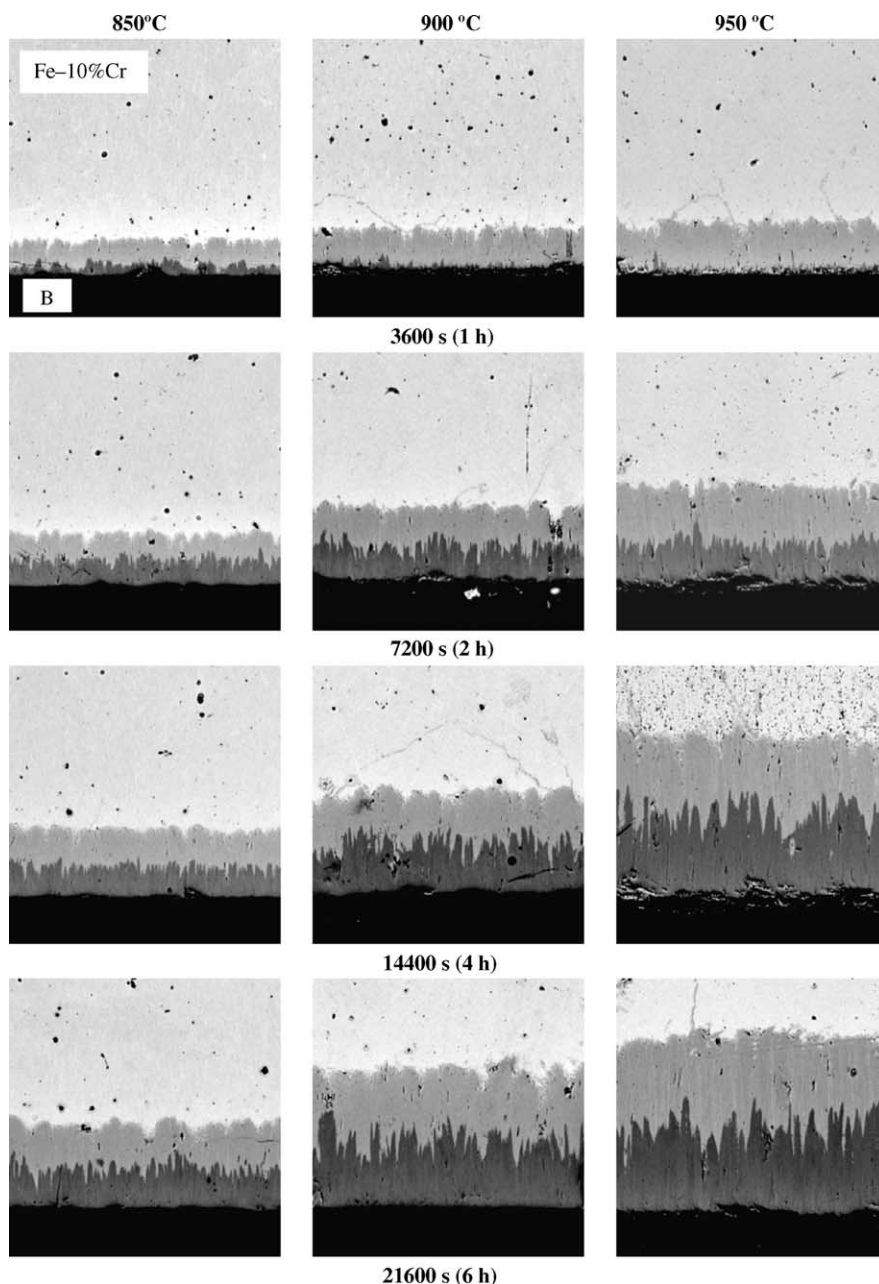


Fig. 2. Backscattered electron images of the Fe–10% Cr alloy–boron interface. The darker layer bordering the boriding agent is the FeB phase, while the brighter layer adjacent to the Fe–Cr alloy base is the Fe<sub>2</sub>B phase.

101 the temperature attained its pre-determined value in 4–5 min  
 102 and was then maintained constant within  $\pm 1^\circ\text{C}$  with the  
 103 help of an automatic thermoregulator VRT-3. The temper-  
 104 ature measurements were carried out using a Pt–PtRh ther-  
 105 mocouple. The experiments were performed at temperatures  
 106 of 850, 900 and  $950^\circ\text{C}$ . Their duration was 3600–43,200 s  
 107 (1–12 h).

108 After the experiment, the Fe–Cr alloy tablet coated with  
 109 boride layers was cut along the cylindrical axis into two un-  
 110 equal parts (7 and 4 mm) using an electric-spark machine.  
 111 The greater part of the tablet was embedded into a cold-  
 112 setting epoxy resin and used to prepare a metallographic

cross-section. The lesser part was used for X-ray diffraction  
 investigations (plain-view samples).

113  
 114  
 115  
 116  
 117  
 118  
 119  
 120  
 121  
 122  
 123  
 124  
 125  
 126  
 127  
 128  
 129  
 130  
 131  
 132  
 133  
 134  
 135  
 136  
 137  
 138  
 139  
 140  
 141  
 142  
 143  
 144  
 145  
 146  
 147  
 148  
 149  
 150  
 151  
 152  
 153  
 154  
 155  
 156  
 157  
 158  
 159  
 160  
 161  
 162  
 163  
 164  
 165  
 166  
 167  
 168  
 169  
 170  
 171  
 172  
 173  
 174  
 175  
 176  
 177  
 178  
 179  
 180  
 181  
 182  
 183  
 184  
 185  
 186  
 187  
 188  
 189  
 190  
 191  
 192  
 193  
 194  
 195  
 196  
 197  
 198  
 199  
 200  
 201  
 202  
 203  
 204  
 205  
 206  
 207  
 208  
 209  
 210  
 211  
 212  
 213  
 214  
 215  
 216  
 217  
 218  
 219  
 220  
 221  
 222  
 223  
 224  
 225  
 226  
 227  
 228  
 229  
 230  
 231  
 232  
 233  
 234  
 235  
 236  
 237  
 238  
 239  
 240  
 241  
 242  
 243  
 244  
 245  
 246  
 247  
 248  
 249  
 250  
 251  
 252  
 253  
 254  
 255  
 256  
 257  
 258  
 259  
 260  
 261  
 262  
 263  
 264  
 265  
 266  
 267  
 268  
 269  
 270  
 271  
 272  
 273  
 274  
 275  
 276  
 277  
 278  
 279  
 280  
 281  
 282  
 283  
 284  
 285  
 286  
 287  
 288  
 289  
 290  
 291  
 292  
 293  
 294  
 295  
 296  
 297  
 298  
 299  
 300  
 301  
 302  
 303  
 304  
 305  
 306  
 307  
 308  
 309  
 310  
 311  
 312  
 313  
 314  
 315  
 316  
 317  
 318  
 319  
 320  
 321  
 322  
 323  
 324  
 325  
 326  
 327  
 328  
 329  
 330  
 331  
 332  
 333  
 334  
 335  
 336  
 337  
 338  
 339  
 340  
 341  
 342  
 343  
 344  
 345  
 346  
 347  
 348  
 349  
 350  
 351  
 352  
 353  
 354  
 355  
 356  
 357  
 358  
 359  
 360  
 361  
 362  
 363  
 364  
 365  
 366  
 367  
 368  
 369  
 370  
 371  
 372  
 373  
 374  
 375  
 376  
 377  
 378  
 379  
 380  
 381  
 382  
 383  
 384  
 385  
 386  
 387  
 388  
 389  
 390  
 391  
 392  
 393  
 394  
 395  
 396  
 397  
 398  
 399  
 400  
 401  
 402  
 403  
 404  
 405  
 406  
 407  
 408  
 409  
 410  
 411  
 412  
 413  
 414  
 415  
 416  
 417  
 418  
 419  
 420  
 421  
 422  
 423  
 424  
 425  
 426  
 427  
 428  
 429  
 430  
 431  
 432  
 433  
 434  
 435  
 436  
 437  
 438  
 439  
 440  
 441  
 442  
 443  
 444  
 445  
 446  
 447  
 448  
 449  
 450  
 451  
 452  
 453  
 454  
 455  
 456  
 457  
 458  
 459  
 460  
 461  
 462  
 463  
 464  
 465  
 466  
 467  
 468  
 469  
 470  
 471  
 472  
 473  
 474  
 475  
 476  
 477  
 478  
 479  
 480  
 481  
 482  
 483  
 484  
 485  
 486  
 487  
 488  
 489  
 490  
 491  
 492  
 493  
 494  
 495  
 496  
 497  
 498  
 499  
 500

The thickness of boride layers was measured using an  
 optical microscope MIM-7 equipped with a HP Photosmart  
 720 camera. The chemical composition of the layers and the

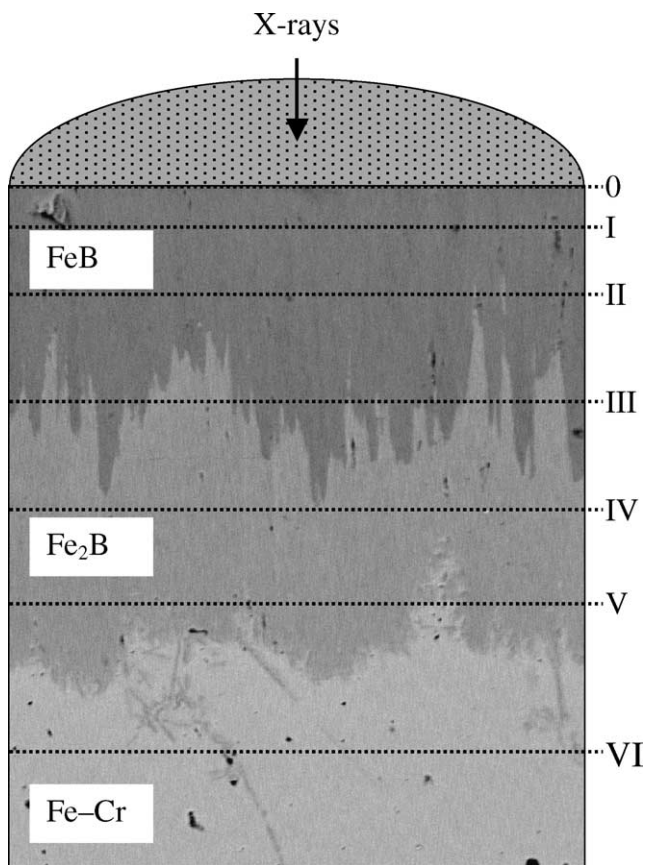


Fig. 3. Scheme of X-ray diffraction experiments.

was repeated at a step of 20–40 μm until the Fe–Cr alloy base was reached (sections II–VI). Seven X-ray diffraction patterns were thus taken on each borided Fe–Cr sample.

Microhardness measurements on metallographic cross-sections were carried out using a PMT-3 tester with the diamond pyramid. The load was 0.98 N (100 g).

Abrasive wear resistance tests were carried out on P180 emery paper tape using an AWRD-5 device. The velocity of movement of the tape was 0.35 m s<sup>-1</sup>, while the gauge length was 27.0 m. The load was 50 N (5.1 kg). The working area of tablet samples was 1 cm<sup>2</sup>. The wear resistance was determined by weighing the samples and measuring their height. Layer-by-layer measurements on the same borided Fe–Cr sample permitted the wear characteristics of different boride phases as well as the alloy base to be determined separately.

### 3. Results and discussion

#### 3.1. Phase identity and chemical composition of boride layers

Two boride phases were found to form as separate layers at the interface between a Fe–10% Cr alloy and boron at 850–950 °C and reaction times up to 12 h (Fig. 2). Layer-by-layer X-ray analysis (Fig. 3) showed the outer layer bordering the boriding agent to be the FeB phase (Table 1), and the inner layer adjacent to the Fe–Cr alloy base to be the Fe<sub>2</sub>B phase (Table 2).

Both layers consist of columnar crystals oriented in the direction of diffusion. Their characteristic feature is a pronounced texture. The strongest reflections are {002} (spacing, *d*=0.148 nm) and, to a lesser extent, {020} (*d*=0.275 nm) for the orthorhombic FeB phase, and {002} (*d*=0.212 nm) for the tetragonal Fe<sub>2</sub>B phase. The change in intensities of those reflections with increasing distance from the surface of a borided Fe–10% Cr alloy tablet is illustrated in Table 3. X-ray investigations were followed by EPMA measurements (Table 4).

Sections 0, I and II of a borided Fe–Cr sample corresponded to the FeB phase. Section III crossed both the FeB and Fe<sub>2</sub>B phases (Figs. 3 and 4). Section IV only crossed the

concentration profiles of the elements in the transition zone between reacting phases were obtained using electron probe microanalyzers JEOL Superprobe 733 and CAMECA Camebax SX50. The beam spot diameter and the phase volume analyzed at each point were estimated to be about 1 μm and 2 μm<sup>3</sup>, respectively.

X-ray diffraction patterns were taken immediately from the surface of tablet samples on a DRON-3 apparatus using Cu Kα radiation. When taking the first pattern, no polishing of a borided Fe–Cr alloy sample was applied (section 0). Then, about 20 μm of a boride layer was removed by grinding and subsequent polishing, and another X-ray diffraction pattern was taken (section I). This procedure

Table 3  
X-ray diffraction data showing preferential directions of growth for the FeB and Fe<sub>2</sub>B phases (see also Figs. 3 and 4)

Phase	<i>hkl</i>	<i>d</i> (nm)	Peak intensity (arbitrary units)						
			0 <sup>a</sup>	I	II	III	IV	V	VI
FeB	020	0.275	88	90	115	35			
	002	0.148	218	2400	2700	1900			
Fe <sub>2</sub> B	002	0.212				400	2700	120	
α-Fe	110	0.201						15	255
	200	0.143							25
	211	0.117							48

<sup>a</sup> Serial numbers of appropriate sections of a borided tablet sample by a plane parallel to its flat surface (section 0, I and so on, deeper into the sample bulk, see Fig. 3).

Table 4  
Averaged Fe, Cr and B contents of reacting phases, found by EPMA measurements on X-ray diffraction samples (see also Figs. 3 and 4)

Section	Content (at.%)			Phase
	Fe	Cr	B	
0	44.1	5.5	50.4	(Fe, Cr)B
I	45.1	5.7	49.2	(Fe, Cr)B
II	43.8	5.2	51.0	(Fe, Cr)B
III <sup>a</sup>	45.1	5.5	49.4	(Fe, Cr)B
	61.1	6.0	32.9	(Fe, Cr) <sub>2</sub> B
IV	58.7	7.5	33.8	(Fe, Cr) <sub>2</sub> B
V	59.3	6.6	34.1	(Fe, Cr) <sub>2</sub> B
VI	89.5	10.5	0.0	(Fe)

<sup>a</sup> Two-phase microstructure (see Fig. 4).

177 FeB phase. The microstructure of section V consisted of the  
178 FeB phase and, to a lesser extent, the alloy base, while that of  
179 section VI was entirely the alloy base. As seen from Table 3,  
180 the larger orientation order is characteristic of the inner portions  
181 of both boride layers compared to their near-interface  
182 portions, in agreement with findings of the other researchers  
183 [1,12].

184 The FeB and Fe<sub>2</sub>B phases dissolve considerable amounts  
185 of chromium (Tables 4 and 5). Its distribution within  
186 the boride layers is rather irregular (Fig. 5). The average  
187 chromium content is 6 ± 1 at.% in the FeB layer and  
188 7 ± 2 at.% in the Fe<sub>2</sub>B layer.

### 189 3.2. Microhardness of boride phases

190 Microhardness, HV, of the FeB layer was found to be  
191 13.0 ± 0.9 GPa, while that of the Fe<sub>2</sub>B layer 11.8 ± 0.8 GPa.  
192 For the Fe–10% Cr alloy base, its value is 1.3 ± 0.1 GPa. A  
193 plot of microhardness values against distance across reacting  
194 phases is shown in Fig. 6. Microhardness is practically constant  
195 within both boride layers and slightly diminishes (by  
196 about 0.1 GPa) in the alloy base with increasing distance in  
197 the range 0–300 μm from the inner boride layer.

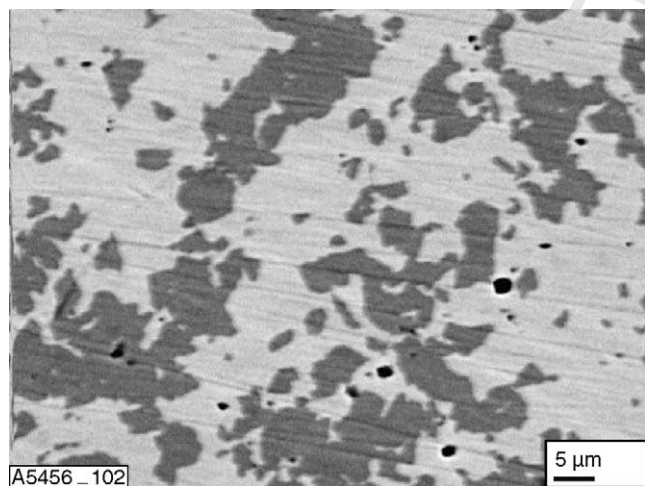


Fig. 4. A plain-view micrograph corresponding to section III in Fig. 3. The darker phase is FeB, while the brighter phase is Fe<sub>2</sub>B. Black spots are holes.

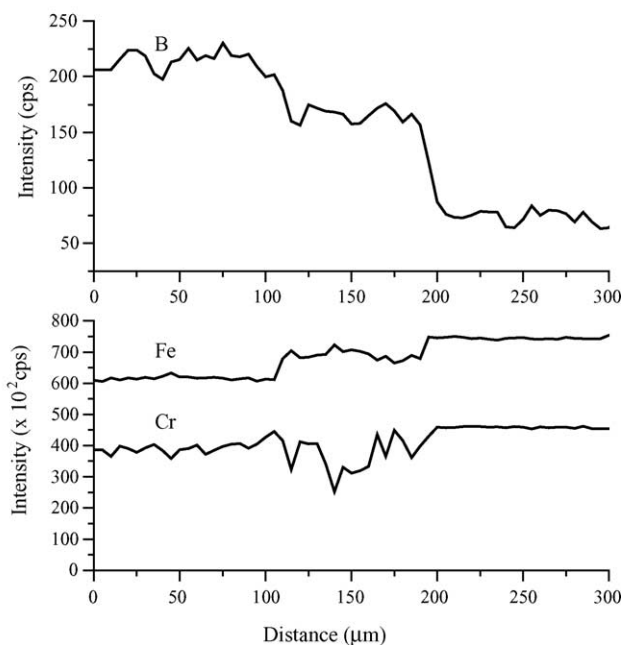
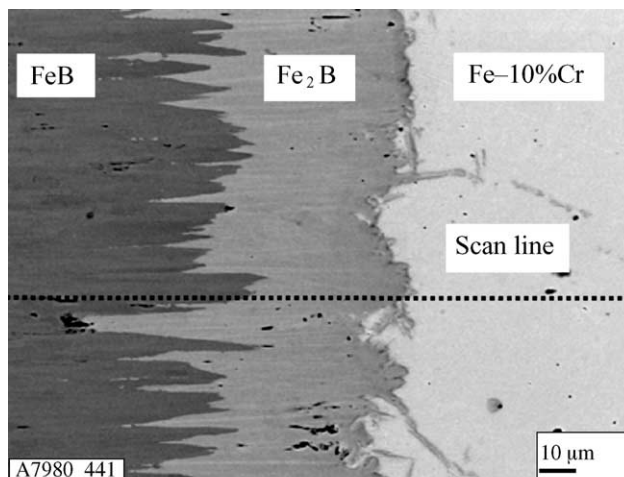


Fig. 5. Microstructure of the transition zone between a Fe–10% Cr alloy and boron and concentration profiles of Fe, Cr and B. Boriding conditions: temperature 950 °C, reaction time 21,600 s (6 h).

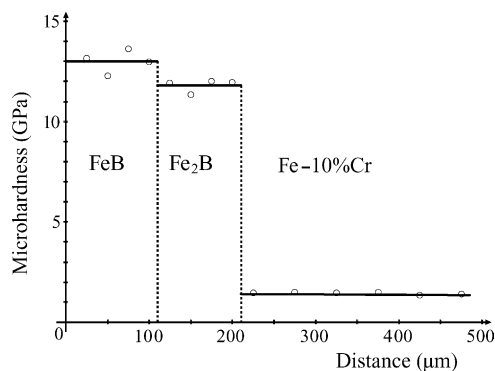


Fig. 6. A plot of microhardness, HV, against distance within the reacting phases. Boriding conditions: temperature 950 °C, reaction time 21,600 s (6 h).

Table 5  
EPMA data for the Fe–10% Cr alloy–boron diffusion zone

Phase	Place of measurement (at distance $l$ away from the alloy–boride layer interface) ( $\mu\text{m}$ )	Content (at.%)			Remarks
		Fe	Cr	B	
Fe–Cr	–100	89.7	10.3	0.0	(Fe)
	–50	89.6	10.4	0.0	
	–30	89.4	10.6	0.0	
	–20	88.1	10.3	1.6	
	–10	89.5	10.5	0.0	
Inner boride layer	10	59.6	7.1	33.3	(Fe, Cr) <sub>2</sub> B
	20	59.7	7.3	33.0	
	30	61.2	6.5	32.3	
	40	58.9	7.8	33.3	
	50	59.4	6.5	34.1	
	60	61.5	5.1	33.4	
	70	59.3	9.1	31.6	
	80	59.0	8.0	33.0	
Outer boride layer	90	44.4	5.9	49.7	(Fe, Cr)B
	100	43.1	5.1	51.7	
	110	44.5	6.3	49.2	
	120	44.7	6.0	49.3	
	130	43.3	5.3	51.4	
	140	44.0	6.3	49.8	
	150	43.2	5.0	51.7	

Temperature 950 °C, reaction time 21,600 s (6 h).

### 3.3. Layer-growth kinetics

Experimental data obtained provide evidence for the sequential rather than simultaneous formation of boride layers, with the Fe<sub>2</sub>B layer occurring first. As seen in Fig. 2, at 900 and 950 °C even a 1 h hold does not yet result in the formation of a continuous layer of the FeB compound over the whole B–Fe<sub>2</sub>B interface. This compound only exists as separate crystals in the Fe<sub>2</sub>B matrix.

After continuous layers of both borides have formed, their subsequent diffusional growth is due to two partial chemical reactions (Fig. 7):



and

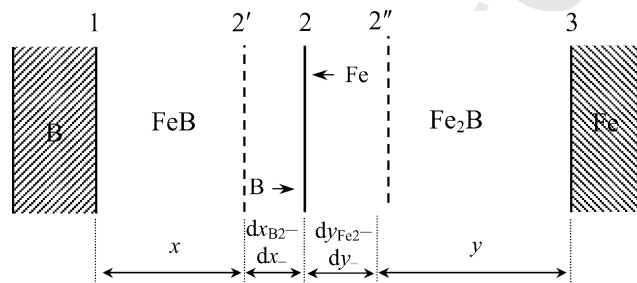


Fig. 7. Schematic diagram to illustrate the growth process of two boride layers under conditions of diffusion control. Both layers thicken at their common interface 2. No reactions take place at interfaces 1 and 3 in view of the lack of appropriate diffusing atoms.

The diffusional growth kinetics of compound layers are usually treated using parabolic equations of the type  $x^2 = 2k_1t$ , where  $x$  is the layer thickness,  $k_1$  the layer growth-rate constant and  $t$  the time [9,13,14]. For sufficiently thick layers, such equations produce a quite satisfactory fit to the experimental data (Fig. 8 and Table 6).

In fact, however, growth kinetics of the FeB and Fe<sub>2</sub>B layers at the diffusional stage of their formation are somewhat more complicated and described by a system of two non-linear equations [10,15]:

$$\frac{dx}{dt} = \frac{k_B}{x} - \frac{rg k_{\text{Fe}}}{p y} \quad (2_1)$$

$$\frac{dy}{dt} = \frac{k_{\text{Fe}}}{y} - \frac{q k_B}{sg x} \quad (2_2)$$

where  $x$  is the FeB layer thickness,  $y$  the Fe<sub>2</sub>B layer thickness,  $k_B$  the FeB layer growth-rate constant,  $k_{\text{Fe}}$  the Fe<sub>2</sub>B layer growth-rate constant,  $g$  the ratio of the molar volumes of the FeB and Fe<sub>2</sub>B compounds,  $p = q = r = 1$  and  $s = 2$ .

Under conditions of diffusion control, both boride layers thicken at their common interface 2, as shown in Fig. 7. The FeB layer grows at the expense of diffusion of the B atoms across its bulk and their subsequent reaction with the Fe<sub>2</sub>B compound. As a result, its thickness increases during  $dt$  by  $dx_{\text{B}_2}$ . The Fe<sub>2</sub>B layer grows at the expense of diffusion of the Fe atoms across its bulk and their further reaction with the FeB compound. During the same time  $dt$ , its thickness increases by  $dy_{\text{Fe}_2}$ . Since the FeB and Fe<sub>2</sub>B compounds are consumed in the formation of each other, the thickness of the FeB layer simultaneously decreases by  $dx_-$ , while that of the Fe<sub>2</sub>B layer by  $dy_-$ . The net change

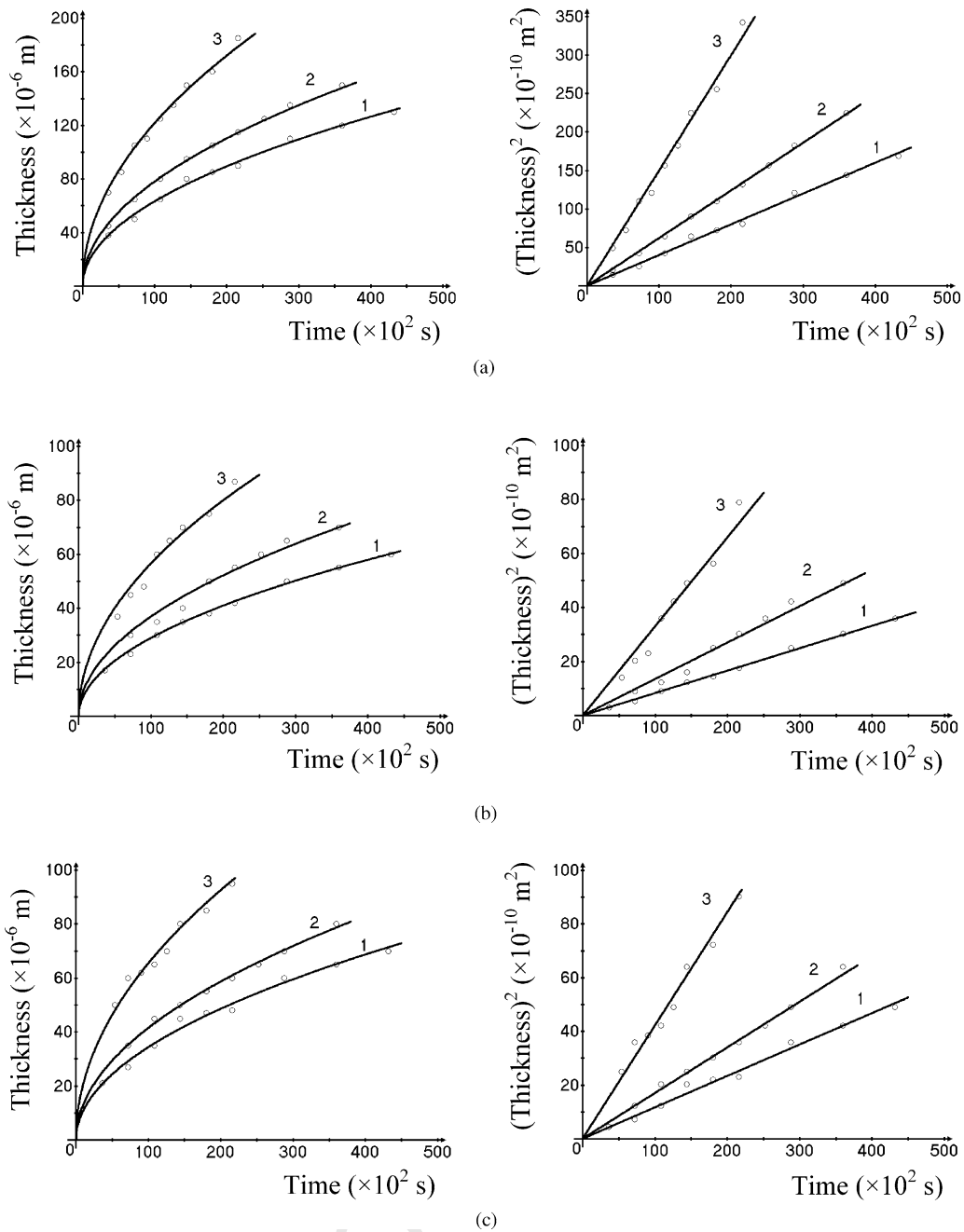


Fig. 8. Plots of layer thickness (left) and squared layer thickness (right) against time for (a) both boride layers, (b) the FeB layer and (c) the Fe<sub>2</sub>B layer at a temperature of 850 °C (line 1), 900 °C (line 2) and 950 °C (line 3).

240 of the FeB layer thickness during  $dt$  is the difference be-  
 241 tween  $dx_{B2}$  and  $dx_-$ , while that of the Fe<sub>2</sub>B layer thick-  
 242 ness is the difference between  $dy_{Fe2}$  and  $dy_-$ . Therefore,  
 243 Eqs. (2<sub>1</sub>) and (2<sub>2</sub>) contain two terms on their right-hand  
 244 parts.

245 An obvious criterion for the applicability of the system  
 246 of Eqs. (2<sub>1</sub>) and (2<sub>2</sub>) is the constancy of  $k_B$  and  $k_{Fe}$  over  
 247 a given range of time, as is the case with both boride lay-  
 248 ers (Table 6). The value of  $g$  necessary for calculations of  
 249  $k_B$  and  $k_{Fe}$  was estimated from the densities of the FeB and  
 250 Fe<sub>2</sub>B compounds ( $6.706 \times 10^3$  and  $7.336 \times 10^3$  kg m $^{-3}$ , re-

spectively [1]) as 0.60. The derivatives were found from the  
 251 experimental layer thickness–time dependences by the nu-  
 252 merical three-point method.  
 253

254 As seen in Table 6, the results of calculations using the  
 255 system of Eqs. (2<sub>1</sub>) and (2<sub>2</sub>) are strongly dependent upon the  
 256 accuracy of measuring layer thicknesses. Approximations of  
 257 experimental data with any suitable analytical functions are  
 258 therefore advisable to obtain more accurate values of  $k_B$  and  
 259  $k_{Fe}$ . For example, the use of parabolic relations to approxi-  
 260 mate the layer thickness–time dependences and then to find  
 261 the derivatives produces another set of values of  $k_B$  and  $k_{Fe}$

Table 6  
Kinetic data for the FeB and Fe<sub>2</sub>B layers formed at the Fe–10% Cr alloy–boron interface

Temperature (°C)	Time (×10 <sup>2</sup> s)	$x$ (×10 <sup>-6</sup> m)			$k_1$ (×10 <sup>-14</sup> m <sup>2</sup> s <sup>-1</sup> )			$k$ (×10 <sup>-13</sup> m <sup>2</sup> s <sup>-1</sup> )	
		Total	FeB	Fe <sub>2</sub> B	Total	FeB	Fe <sub>2</sub> B	$k_B$	$k_{Fe}$
850	36	38	17	21	20.0	4.0	6.1		
	72	50	23	27	17.4	3.7	5.1	3.0	5.0
	108	65	30	35	19.5	4.0	5.7	3.4	5.6
	144	80	35	45	22.2	4.2	7.0	2.6	4.8
	180	85	38	47	20.1	4.0	6.1	1.7	2.7
	216	90	42	48	18.8	4.1	5.3	2.5	4.0
	288	110	50	60	21.0	4.3	6.3	4.1	6.6
	360	120	55	65	20.0	4.2	5.9	2.6	3.6
432	130	60	70	19.6	4.2	5.7			
900	36	45	45		28.1				
	72	65	30	35	29.3	6.3	8.5	5.4	8.9
	108	80	35	45	29.6	5.7	9.4	3.3	6.0
	144	95	40	50	31.3	5.6	8.7	4.2	6.9
	180	105	50	55	30.6	6.9	8.4	5.2	7.6
	216	115	55	60	30.6	7.0	8.3	4.4	6.6
	252	125	60	65	31.0	7.1	8.4	4.8	7.1
	288	135	65	70	31.6	7.3	8.5	4.4	6.6
360	150	70	80	31.3	6.8	8.9			
950	36	70	70		68.1				
	54	85	35	50	66.9	11.3	23.1	13.1	26.1
	72	105	45	60	76.6	14.1	25.0	9.0	16.4
	90	110	48	62	67.2	12.8	21.4	8.6	14.1
	108	125	60	65	72.3	16.7	19.6	13.0	18.3
	126	135	65	70	72.3	16.8	19.4	12.3	18.8
	144	150	70	80	78.1	17.0	22.2	10.4	17.1
	180	160	75	85	71.1	15.6	20.1	10.8	16.4
216	185	90	95	79.2	18.8	20.9			

(Table 7). Comparing these with the average values of  $k_B$  and  $k_{Fe}$  found numerically from the experimental points, it may be concluded that both sets of the constants agree fairly well, providing evidence for the validity of the analytical treatment proposed.

The temperature dependence of the layer growth-rate constants is described in the 850–950 °C range by the following equations of the Arrhenius type:

$k_1 = 3.89 \times 10^{-7} \exp(-150.6 \text{ kJ mol}^{-1}/RT) \text{ m}^2 \text{ s}^{-1}$  for the FeB layer.

$k_1 = 3.46 \times 10^{-7} \exp(-146.4 \text{ kJ mol}^{-1}/RT) \text{ m}^2 \text{ s}^{-1}$  for the Fe<sub>2</sub>B layer.

$k_1 = 13.22 \times 10^{-7} \exp(-147.5 \text{ kJ mol}^{-1}/RT) \text{ m}^2 \text{ s}^{-1}$  for both boride layers.

$$k_B = 2.16 \times 10^{-6} \exp(-149.8 \text{ kJ mol}^{-1}/RT) \text{ m}^2 \text{ s}^{-1}.$$

$$k_{Fe} = 2.79 \times 10^{-6} \exp(-147.5 \text{ kJ mol}^{-1}/RT) \text{ m}^2 \text{ s}^{-1}.$$

### 3.4. Degradation of boride layers during annealing in the absence of boriding media

Annealing of a borided Fe–Cr sample (Fig. 9a) in the absence of boriding media results in a decrease of the thickness of the FeB layer and an appropriate increase of the thickness of the Fe<sub>2</sub>B layer. As seen in Fig. 9b, 6 h annealing at 950 °C causes the full disappearance of the FeB layer, about 90 μm thick initially. Further annealing leads to disintegration of the Fe<sub>2</sub>B layer into separate grains. As evidenced in Fig. 9c, grain-boundary diffusion

Table 7  
Average values of layer growth-rate constants

Temperature (°C)	$k_1$ (×10 <sup>-14</sup> m <sup>2</sup> s <sup>-1</sup> )			$k$ (×10 <sup>-13</sup> m <sup>2</sup> s <sup>-1</sup> ) from experimental points		$k$ (×10 <sup>-13</sup> m <sup>2</sup> s <sup>-1</sup> ) from approximated dependences	
	Total	FeB	Fe <sub>2</sub> B	$k_B$	$k_{Fe}$	$k_B$	$k_{Fe}$
850	19.8	4.1	5.9	2.8	4.6	2.5	4.2
900	30.4	6.6	8.6	4.5	7.1	4.0	6.3
950	72.4	15.4	21.4	11.0	18.2	9.4	15.4

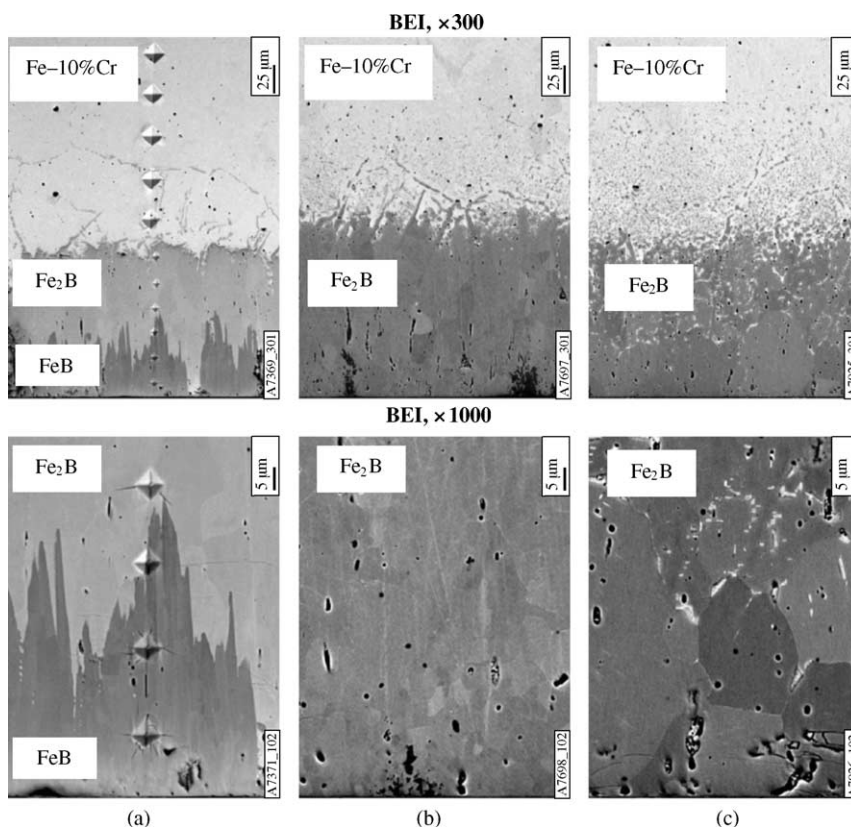


Fig. 9. Degradation of boride layers during vacuum annealing at a temperature of 950 °C in the absence of boriding media: (a) as-received condition, (b) 6 h annealing and (c) 12 h annealing. BEI: backscattered electron image, magnification 300× and 1000×.

288 appears to play a significant, if not decisive, role in this pro- 296  
 289 cess. 289

290 3.5. Abrasive wear resistance of boride layers

291 Boriding the Fe–Cr alloy tablets for abrasive wear resis- 296  
 292 tance tests was performed at 950 °C for 6 h, producing the (Fe, 297  
 293 Cr)B and (Fe, Cr)<sub>2</sub>B layers of approximately equal thickness 298  
 294 (180–200 μm in total). Three consecutive tests were carried 299  
 295 out on each borided Fe–Cr sample, with each test along a fresh 300  
 301  
 302  
 303  
 304  
 305

track on emery paper. The results obtained are presented in 296  
 Table 8, where the data for a non-borided Fe–Cr sample are 297  
 also given for comparison. 298

The wear resistance of the (Fe, Cr)B layer, found from 299  
 mass loss measurements, is at least 10 times greater than that 300  
 of the alloy base. Somewhat lesser resistance of its outermost 301  
 portions, compared to deeper ones consisting of both boride 302  
 phases, is due to the greater amount of cracks in the near- 303  
 surface region. The (Fe, Cr)<sub>2</sub>B layer yields about a 5-fold 304  
 increase in wear resistance of an Fe–10% Cr alloy. 305

Table 8  
 Results of abrasive wear resistance tests of borided Fe–Cr alloy samples

Borided sample number	Test number	$\Delta m$ (g) <sup>a</sup>	$\Delta h$ (mm)	Phase
108	1	0.03470	0.060	(Fe, Cr)B
	2	0.02740	0.050	(Fe, Cr)B + (Fe, Cr) <sub>2</sub> B
	3	0.06920	0.090	(Fe, Cr) <sub>2</sub> B
109	1	0.03415	0.055	(Fe, Cr)B
	2	0.02485	0.045	(Fe, Cr)B + (Fe, Cr) <sub>2</sub> B
	3	0.06925	0.095	(Fe, Cr) <sub>2</sub> B
110	1	0.03995	0.060	(Fe, Cr)B
	2	0.02585	0.045	(Fe, Cr)B + (Fe, Cr) <sub>2</sub> B
	3	0.06605	0.085	(Fe, Cr) <sub>2</sub> B
		0.39500	0.50	Non-borided Fe–Cr

Boriding conditions: temperature 950 °C, reaction time 21,600 s (6h).

<sup>a</sup>  $\Delta m$  and  $\Delta h$  are changes in mass and height, respectively, of samples.

#### 4. Conclusions

Two boride phases FeB and Fe<sub>2</sub>B form separate layers at the interface between a Fe–10% Cr alloy and boron at 850–950 °C and reaction times up to 12 h. The average content of chromium is around 6 at.% in the FeB layer and 7 at.% in the Fe<sub>2</sub>B layer. Its distribution within the boride layers is rather irregular.

The characteristic feature of both layers is a pronounced texture. The strongest reflections are {002} and {020} for the orthorhombic FeB phase and {002} for the tetragonal Fe<sub>2</sub>B phase.

Formation of boride layers is sequential rather than simultaneous, with the Fe<sub>2</sub>B layer occurring first. After sufficiently thick layers of both borides have formed, their further diffusional growth kinetics are close to parabolic. Alternatively, layer-growth kinetics can be described by a system of non-linear differential equations, also producing a good fit to the experimental data.

Annealing of a borided Fe–Cr sample in the absence of boriding media results in the disappearance of the FeB layer and then in the disintegration of the Fe<sub>2</sub>B layer into separate grains. Grain-boundary diffusion appears to play a significant, if not decisive, role in this process.

Microhardness values are 13.0 GPa for the FeB layer, 11.8 GPa for the Fe<sub>2</sub>B layer and 1.3 GPa for the Fe–10% Cr alloy base. Microhardness is constant within both boride layers and slightly diminishes (by about 0.1 GPa) in the alloy base with increasing distance in the range of 0–300 μm from the inner boride layer.

The abrasive wear resistance of the (Fe, Cr)B layer, found from mass loss measurements, is at least 10 times greater than that of the alloy base. The (Fe, Cr)<sub>2</sub>B layer yields about a 5-fold increase in the wear resistance of an Fe–10% Cr alloy.

#### Acknowledgements

This investigation was supported in part by the STCU grant no. 2028. The authors thank V.G. Khoruzha, V.R. Sidorko, K.A. Meleshevich and A.V. Samelyuk for their help in conducting the experiments and carrying out the necessary analyses.

#### References

- [1] L.G. Voroshnin, L.S. Lyakhovich, *Borirovaniye stali*, Metallurgiya, Moskva, 1978 (in Russian).
- [2] H. Kunst, H. Schroll, R. Luetje, K. Wittel, E. Lugscheider, T. Weber, H.R. Eschnauer, C. Raub, Surface treatment, in: *Ullmann's Encyclopedia of Industrial Chemistry*, vol. A16, Verlag Chemie, Weinheim, 1991, p. 427.
- [3] A.K. Sinha (Ed.), *Metals Handbook*, ASM International, Metals Park, OH, 1982, p. 844.
- [4] M. Hansen, K. Anderko, *Constitution of Binary Alloys*, second ed., McGraw-Hill, New York, 1958, p. 249.
- [5] A.E. Vol, *Stroeniye i svoystva dvoynikh metallicheskih system*, 1, Fizmatgiz, Moskva, 1962, p. 679 (in Russian).
- [6] T.B. Massalski, J.L. Murray, L.H. Bennett, H. Baker (Eds.), *Binary Alloy Phase Diagrams*, vol. 1, American Society of Metals, Metals Park, OH, 1986, p. 351.
- [7] H. Okamoto, *J. Phase Equilib. Diffusion* 25 (2004) 297–298.
- [8] J. Brandstötter, W. Lengauer, *J. Alloys Compd.* 262–263 (1997) 390–396.
- [9] K.P. Gurov, B.A. Kartashkin, Yu.E. Ugaste, *Vzaimnaya diffusiya v mnogofaznikh metallicheskih sistemakh*, Nauka, Moskva, 1981 (in Russian).
- [10] V.I. Dybkov, *Reaction Diffusion and Solid State Chemical Kinetics*, The IPMS Publications, Kyiv, 2002.
- [11] S.S. Gorelik, L.N. Rastorguev, Yu.A. Skakov, *Rentgenograficheskiy i elektronno-opticheskiy analiz, prilozheniya*, Metallurgiya, Moskva, 1970, p. 29 (in Russian).
- [12] M. Carbucicchio, G. Palombarini, *J. Mater. Sci. Lett.* 6 (1987) 1147–1149.
- [13] W. Seith, *Diffusion in Metallen*, Springer, Berlin, 1955.
- [14] K. Hauffe, *Reaktionen in und an festen Stoffen*, Springer, Berlin, 1955.
- [15] O.V. Dybkov, V.I. Dybkov, *J. Mater. Sci. Lett.* 39 (2004) 6615–6617.